











Observation of entanglement in a cold atom analog of cosmological preheating

Victor Gondret ^{1,*} Clothilde Lamirault ¹ Rui Dias ¹ Léa Camier ¹ Amaury Micheli ² Charlie Leprince ¹
 Quentin Marolleau ^{1,†} Jean-René Rullier,¹ Scott Robertson ³ Denis Boiron ^{1,‡} and Christoph I. Westbrook ^{1,§}

¹*Université Paris-Saclay, Institut d'Optique Graduate School, CNRS, Laboratoire Charles Fabry, 91127, Palaiseau, France*

²*RIKEN Interdisciplinary Theoretical and Mathematical Sciences (iTHEMS), Wako, Saitama 351-0198, Japan*

³*Institut Pprime, CNRS – Université de Poitiers – ISAE-ENSMA, TSA 51124, 86073 Poitiers Cedex 9, France*

We observe entanglement between collective excitations of a Bose-Einstein condensate in a configuration analogous to particle production during the preheating phase of the early universe. In our setup, the oscillation of the inflaton field is mimicked by the transverse breathing mode of a cigar-shaped condensate, which parametrically excites longitudinal quasiparticles with opposite momenta. After a short modulation period, we observe entanglement of these pairs which demonstrates that vacuum fluctuations seeded the parametric growth, confirming the quantum origin of the excitations. As the system continues to evolve, we observe a decrease in correlations and a disappearance of non-classical features, pointing towards future experimental probes of the less understood interaction-dominated regime.

In quantum field theory, particles are identified with excitations of fields. Even in a vacuum, fields are subject to quantum fluctuations, which can be amplified to create particles. This phenomenon plays a crucial role in astrophysics and cosmology and is known as spontaneous particle production, to distinguish it from its stimulated counterpart seeded by classical fluctuations. It is the underlying mechanism behind black hole evaporation via Hawking radiation [1], the generation of primordial cosmological inhomogeneities during inflation [2], and the generation of particles in an empty post-inflationary universe, a phenomenon known as preheating [3]. However, a direct observation of these phenomena in the cosmological context is currently out of reach [4–6].

Beginning in 1981 [4], a field of study has developed in which fluids host analogs of the above phenomena. Unruh showed that, in the presence of a strong coherent background, the excitations of a fluid, or *quasiparticles*, can be treated using the same formalism as particles in a curved spacetime. Following this idea, analogs of Hawking radiation [7–13], the cosmological redshift [14], quasiparticle production in time-varying geometries [15–17], and false-vacuum decay [18] have been realized among others [19]. However, the entanglement between the produced excitations, a signature of their quantum rather than classical origin, is fragile and elusive, and has only been probed in a few experiments. In Bose-Einstein condensates (BEC), these experiments involved analog Hawking radiation [9] or a sudden quench [20, 21]. In photonic systems, time-modulated boundary conditions produced evidence of spontaneous amplification in a configuration analogous to the dynamical Casimir effect [22, 23].

In this work, we report the observation of entangled, parametrically excited, collective modes in a BEC in an analog to cosmological preheating. In preheating, oscillations of a hypothetical field, known as the “inflaton”, parametrically create particles in other, previously empty fields. The role of the inflaton is played by the transverse degrees of freedom of the elongated BEC, which are coupled to the longitudinal ones: transverse oscillations parametrically excite longitudinal modes. The low thermal population of these modes ensures that their growth is seeded largely by vacuum fluctua-

tions, which results in an entangled two-mode state. This type of parametric amplification has been studied in quantum fluids and referred to as Faraday wave generation [24–29], but the cited experiments did not witness entanglement. In our case, the observation is made possible by a very low BEC temperature, which enables an investigation in the low occupation number regime. We make two-particle correlation measurements and use recent theoretical advances linking these correlations to entanglement certification [30].

Experiment – A BEC containing about 3 000 metastable helium atoms in the 2^3S_1 , $m_S = 1$ state is trapped in a crossed optical dipole trap [31], see Fig. 1(a). The trapping frequencies are $\omega_\perp/2\pi = 930(20)$ Hz in the radial direction and $\omega_z/2\pi = 40(2)$ Hz in the vertical, axial direction. In an elongated homogeneous cloud, longitudinal collective excitations with momentum q have an energy $\hbar\omega_q$ given by the Bogoliubov dispersion relation [32]

$$\hbar\omega_q = \sqrt{c_{1D}^2 q^2 + \left(\frac{q^2}{2m}\right)^2} \quad (1)$$

where c_{1D} is the longitudinal sound speed, m the atomic mass, and \hbar the reduced Planck constant. A periodic modulation of the sound speed parametrically produces correlated pairs of quasiparticles at momenta $\pm p$, whose frequency $\omega_{\pm p}$ is half the modulation frequency [24–29]. The dynamics can be modeled as a two-mode squeezing operation on the $\pm p$ quasiparticle modes, which can become entangled depending on the initial temperature of the cloud, the thermal damping of the quasiparticles, and the strength of the modulation [33]. In a harmonic trap, momentum states are not the exact eigenmodes of the system, but the physics at play is not expected to change significantly [34].

The periodic modulation of c_{1D} is achieved by varying the power of the dipole trap $\mathcal{P}_{\text{las}} \propto (1 + A \sin 2\omega_\perp t)$. This excites the BEC transverse breathing mode, whose radius $\sigma_{\text{BEC}} \propto 1/c_{1D}$ oscillates at $2\omega_\perp$ [35]. The amplitude of the breathing depends on the modulation amplitude A and its duration, which is kept constant at 4 modulation periods in this work. After the modulation, the trap remains on for a hold

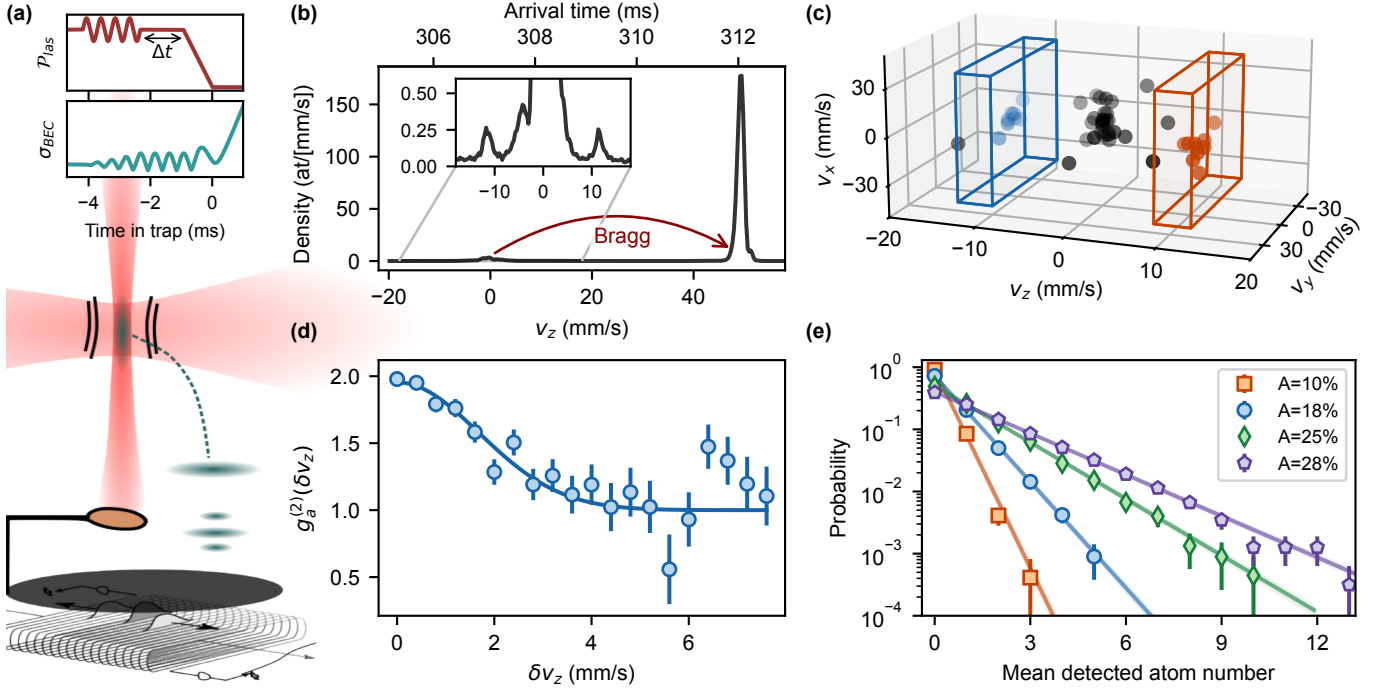


FIG. 1. (a) Diagram of the crossed dipole trap and the MCP detector. The breathing mode of a cigar-shaped BEC is excited for 4 periods by modulating the laser power (top inset, P_{las}). The BEC is held in the trap for a hold time Δt during which its radius σ_{BEC} continues to oscillate (second inset). The trap laser is ramped down in 1 ms to map the collective excitations onto individual atoms (see text). (b) The position and arrival time of individual atoms is recorded, and converted to an initial velocity. Sidebands are visible at ± 11.7 mm/s. A Bragg diffraction pulse shifts more than 97% of the BEC atoms to later times to avoid saturating the detector in the vicinity of the excitations. (c) A single shot showing the excitations in a 3D velocity space. Each dot represents a single atom. The blue and red boxes show the position and size of a typical analysis volume or “voxel”. (d) Auto-correlation function of the measured sideband velocities giving an estimate of the longitudinal mode size and showing its thermal nature. (e) Probability distribution in a single voxel for different modulation depths A . The lines show the probability distribution in Eq. (3) computed from the mean *detected* atom number.

time Δt during which the transverse radius σ_{BEC} continues to oscillate at $2\omega_{\perp}$, see the inset of Fig. 1(a). A peculiar feature of the breathing mode in an elongated cloud is its low damping rate [36] caused by the suppression of Landau damping mechanisms, as both the thermal cloud and the BEC oscillate in phase [37].

After the excitation process, the transverse confinement is ramped down in 1 ms after which the longitudinal confinement is also switched off. This ramp is sufficiently slow to ensure that the collective excitations are mapped onto the atoms by a process referred to as phonon evaporation [38, 39]. During the free fall, these atoms fly away from the BEC, appearing as sidebands in the time-of-flight spectrum relative to the unperturbed condensate when they reach a microchannel plate (MCP) detector, see Fig. 1(b). The MCP detector identifies the arrival time and position of individual atoms with a quantum efficiency which we estimate to be 25(5)%. The detector is located 46 cm below the trap, sufficiently far that the arrival times and positions accurately reflect the atomic velocities when the trap was turned off.

The MCP is shielded from the vertical laser by a metal disc, requiring the atoms to be deflected towards the unshielded region. This is achieved by a 12 μs stimulated Raman transi-

tion which transfers the atoms to the magnetically insensitive $m_S = 0$ state and imparts a transverse velocity of 42 mm/s. In addition, to prevent the saturation of the MCP caused by the high atomic flux from the BEC, a temporally shaped, velocity-selective Bragg pulse, applied 1 ms after the Raman pulse, shifts the BEC to later times thus removing 97% of the BEC atoms from the region where we detect the excitations [40]. A typical single shot velocity reconstruction is shown in Fig. 1(c) where each dot represents an individual atom. The blue and red boxes show the position and size of a typical analysis volume or “voxel”.

Single mode statistics – A typical one-dimensional velocity profile, averaged over 2,000 experimental realizations, is shown in the inset of Fig. 1(b). A Gaussian fit to the sideband density profiles yields typical standard deviations of $\sigma_{\perp} \sim 8$ mm/s in the transverse direction and $\sigma_z \sim 0.8$ mm/s longitudinally. To compare these scales against that of a single collective excitation mode, we construct a histogram of velocity differences between atom pairs. This allows us to compute the normalized two-body auto-correlation function [41]

$$g_a^{(2)}(\delta \mathbf{v}) = \int_{\Omega} \frac{\langle \hat{n}_{\mathbf{v}-\delta \mathbf{v}} \hat{n}_{\mathbf{v}+\delta \mathbf{v}} \rangle}{\langle \hat{n}_{\mathbf{v}+\delta \mathbf{v}} \rangle \langle \hat{n}_{\mathbf{v}-\delta \mathbf{v}} \rangle} d^3 \mathbf{v}, \quad (2)$$

where \hat{n} is the atom number operator, the colons “:” refer

to normal ordering and the integration volume Ω excludes the residual condensate [42]. The sidebands exhibit bunching within a momentum linewidth inversely proportional to the source size in each spatial direction [34, 43]. We show in Fig. 1(d) the auto-correlation function $g_a^{(2)}$ along the z direction. A Gaussian fit to this peak gives a standard deviation of 1.7(1) mm/s, which we interpret as the characteristic momentum width of a single mode [43]. A similar analysis along the transverse direction yields a standard deviation of 9(1) mm/s. Our excitation thus mainly addresses pairs of single modes.

To probe the statistics of these excitations more precisely, a voxel in momentum space is defined—illustrated in Fig. 1(c)—with a longitudinal extent equal to the mode width of 1.7 mm/s, but without transverse selection. The resulting atom number distribution is plotted in Fig. 1(e) for various modulation amplitudes A , corresponding to different mean atom numbers. Tracing over one mode of a two-mode squeezed state—such as the one we expect to generate—results in a thermal density matrix $\sum_{i=0}^{\infty} P_i(n)|i\rangle\langle i|$ [44, 45] where the atom number distribution is given by

$$P_i(n) = \frac{n^i}{(1+n)^{i+1}} \quad (3)$$

and n is the mean detected atom number. In Fig. 1(e), P_i is shown to agree remarkably well with experimentally measured distributions. The thermal character of the state is corroborated by Fig. 1(d) showing that the value of $g_a^{(2)}(\delta v_z = 0)$ approaches 2 [45].

Entanglement – Two-mode entanglement in bosonic systems can be directly inferred from number correlations, provided the underlying quantum state remains Gaussian [30]. Within the Bogoliubov framework, the condensate is treated as a classical background that serves as a particle reservoir for collective excitations. The Hamiltonian is then quadratic, describing non-interacting quasiparticles and thus preserving the Gaussianity of the initial thermal states [39]. This approximation remains valid as long as the condensate depletion is small. The data in Fig. 1(b) confirms the small depletion.

The normalized two-body cross-correlator of a zero-mean Gaussian state can be expanded using Wick's theorem [46], yielding

$$g_{\pm}^{(2)} = \frac{\langle \hat{a}_+^\dagger \hat{a}_+^\dagger \hat{a}_+ \hat{a}_- \rangle}{n_+ n_-} = 1 + \frac{|\langle \hat{a}_+ \hat{a}_- \rangle|^2}{n_+ n_-} + \frac{|\langle \hat{a}_+ \hat{a}_+^\dagger \rangle|^2}{n_+ n_-}, \quad (4)$$

where \hat{a}_{\pm} are the annihilation operators for the positive and negative momentum sideband modes, and $n_{\pm} = \langle \hat{a}_{\pm}^\dagger \hat{a}_{\pm} \rangle$ denote their respective mean occupations. In our experiment, the thermal statistics exhibited by each mode imply that they have zero mean ($\langle \hat{a}_{\pm} \rangle = 0$), and are not single-mode squeezed ($\langle \hat{a}_{\pm}^2 \rangle = 0$) [47], validating the expansion of Eq. (4). In Ref. [30] we have shown that, for such a Gaussian state, the value of $g_{\pm}^{(2)}$ is an entanglement witness irrespective of the value of $\langle \hat{a}_+ \hat{a}_-^\dagger \rangle$. Entanglement is certified whenever $g_{\pm}^{(2)}$ exceeds a threshold which depends on the mode populations. This threshold is shown as the red line in Fig. 2(b).

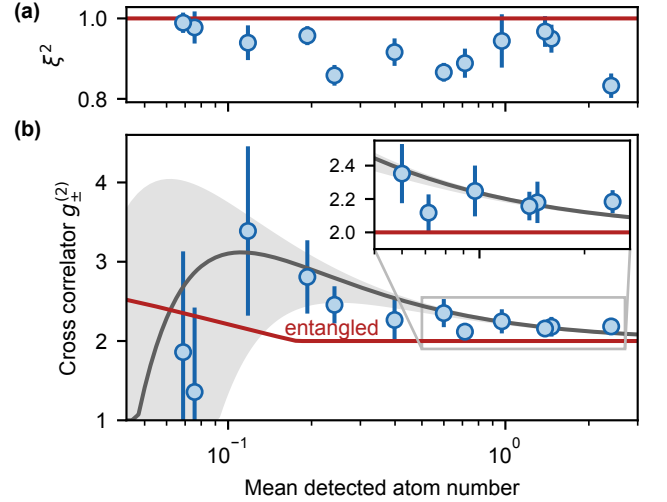


FIG. 2. Relative number squeezing (a) and two-body correlator (b) as a function of the mean *detected* atom number, for modulation amplitudes between $A = 3$ and 28%. The hold time Δt was fixed at 1.6 ms (3 breathing periods). The red line indicates unity (a) and the threshold for the entanglement witness of Ref. [30] in panel (b), assuming a quantum efficiency of 25%. The gray curve shows the expected value assuming a two-mode squeezed thermal state with an initial temperature of 25(5) nK and a quantum efficiency of 25%. The width of the gray band reflects the uncertainty in the temperature. Error bars denote one standard deviation uncertainty and are computed using a bootstrap analysis.

The measured cross-correlator between opposite momenta $g_{\pm}^{(2)}$ is also shown in Fig. 2(b) as a function of the mean detected atom number. This is done by varying the modulation amplitude A by 3 to 28%, fixing the hold time to 3 breathing periods. Ideally, the value of $g_{\pm}^{(2)}$ should be computed in the limit of vanishing voxel size [43]. Here, $g_{\pm}^{(2)}$ is computed between voxels with a transverse size Δv_{\perp} , which matches the fitted full width at half maximum of the transverse density profile, and a longitudinal size of $\Delta v_z = 1.4$ mm/s. This size is smaller than the correlation length to mainly pick out a single mode, yet large enough to ensure sufficient signal-to-noise. On the horizontal axis, the plotted population refers to the average number of detected atoms in the two sideband voxels [48]. We see that the two modes are entangled for a large range of mean detected atom numbers. Assuming that the modes were initially unentangled, this entanglement demonstrates that we successfully created quasiparticles from the vacuum.

Two-mode squeezing model – We now discuss additional checks to demonstrate that the system exhibits the phenomenology expected in our analog preheating picture. First, we compare the observed correlations with those predicted for parametric pair creation in a homogeneous background from modes initially in thermal states. Within the Bogoliubov approximation, the two-mode state remains Gaussian, and we have $\langle \hat{a}_+ \hat{a}_-^\dagger \rangle = 0$ on account of the homogeneity [39]. The

two-mode state is fully described by the sideband populations n_{\pm} and the anomalous correlator $|\langle \hat{a}_+ \hat{a}_- \rangle|$, with [33]

$$\begin{aligned} 2n_{\pm} &= (2n_{\text{th}}^{(\text{in})} + 1) \cosh(2r) - 1, \\ 2|\langle \hat{a}_+ \hat{a}_- \rangle| &= (2n_{\text{th}}^{(\text{in})} + 1) \sinh(2r), \end{aligned} \quad (5)$$

where r is the squeezing parameter [49] and $n_{\text{th}}^{(\text{in})} = 1/(e^{\hbar\omega_{\perp}/k_B T} - 1)$ is the initial thermal occupation of each mode at energy $\hbar\omega_{\perp}$. Entanglement occurs when $|\langle \hat{a}_+ \hat{a}_- \rangle|^2 > n_+ n_-$ [50]. Since $\langle \hat{a}_+ \hat{a}_-^{\dagger} \rangle = 0$ here, by Eq. (4) this is equivalent to $g_{\pm}^{(2)} > 2$ regardless of the mode occupation (i.e., in this model the equivalent of the red line in Fig. 2(b) is a horizontal line at the value 2). The measured temperature 25(5) nK corresponds to $n_{\text{th}}^{(\text{in})} = 0.18(8)$, which corresponds to a detected thermal population of 0.04(2). The low temperature is key to detecting entanglement using our witness. For larger $n_{\text{th}}^{(\text{in})}$ we could still detect entanglement in principle but only at the expense of a larger gain and lower maximal value of $g_{\pm}^{(2)}$ which would be harder to distinguish from the value 2. In Fig. 2(b), the gray band shows the theoretical prediction of this two-mode squeezed thermal state model, assuming a quantum detection efficiency of 25% and our measured temperature. Measured correlations fall within this area and are thus compatible with the expectations of a two-mode squeezed state.

Second, the normalized variance $\xi^2 = \text{var}(n_+ - n_-)/(n_+ + n_-)$ provides a slightly different and complementary way to characterize the state of the produced quasiparticles. The variance is a non-classical signature which does not depend on the Gaussianity of the state nor on its two-mode nature. Thus, we improve the signal-to-noise ratio by choosing large voxels centered on each sideband [51, 52]. The results are shown in Fig. 2(a). At all but the lowest mode populations, the measured values of ξ^2 fall below shot noise level $\xi^2 = 1$, confirming the non-classical nature of the state [53].

Time evolution – We investigate the time evolution by fixing the modulation amplitude and varying the hold time. The results are shown in Fig. 3 for amplitudes of 18% (orange circles) and 25% (green squares). The mean quasiparticle population in the excited modes, shown in Fig. 3(a), exhibits exponential growth, consistent with expectations from parametric resonance [54] and our two-mode squeezed thermal state model [55], see Eq. (5). The corresponding evolution of the normalized two-body correlator $g_{\pm}^{(2)}$ is shown in Fig. 3(b) and the normalized variance between the two modes is shown in the inset of the figure. As the hold time Δt increases, $g_{\pm}^{(2)}$ gradually approaches the value 2. This behavior is easily understood: although the anomalous correlation $|\langle \hat{a}_+ \hat{a}_- \rangle|$ increases with time, the ratio $|\langle \hat{a}_+ \hat{a}_- \rangle|^2/(n_+ n_-)$ decreases as the population grows, leading to a decrease of $g_{\pm}^{(2)}$. On the other hand, for hold times larger than 3 ms, the correlator begins to fall below 2 while the normalized number variance exceeds unity, a behavior not captured by Eq. (5) or its dissipative extension [54, 56]. In this regime, our entanglement witness is no longer satisfied and we cannot infer entanglement. The

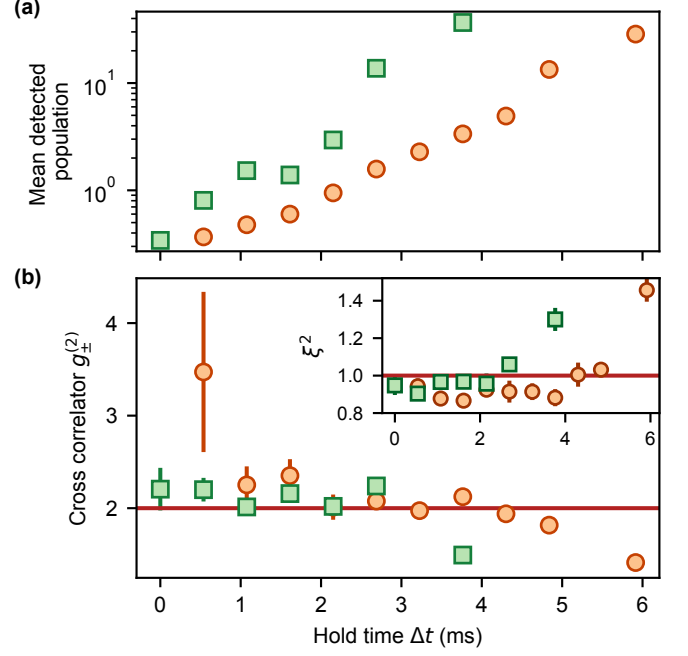


FIG. 3. Plot of the mean detected population (a) and the cross-correlator (b) as a function of the hold time Δt . Data is shown for two different modulation depths (orange circles 18%, green squares 25%). The inset shows the normalized variance. It is seen that at long times one cannot infer the existence of any entanglement. Error bars denote one standard deviation uncertainty and are computed using a bootstrap analysis.

onset of this apparent loss of entanglement for the two modulation amplitudes occurs for similar mode populations.

As suggested in Ref. [57], this apparent loss of entanglement could indicate the onset of a late-time regime where higher order quasi-particle interactions become relevant and a richer phenomenology emerges, *e.g.* decoherence of the resonant modes [57], secondary spectral peaks as observed in similar experiments in hydrodynamic systems [58], or loss of Gaussianity [59, 60]. All these phenomena can be seen steps on the path towards thermalization for which we may be able to draw analogies to “reheating” in the cosmological era when the Universe transitions to a thermal state. Future work will investigate these effects.

Data availability – The data that support the findings of this manuscript are available in a public Zenodo repository at [61].

ACKNOWLEDGMENTS

We acknowledge David Clément and Nicolas Pavloff for their careful reading of the manuscript and Maxime Jacquet for fruitful discussions. A. M. thanks all iTHEMS members, in particular Tsukasa Tada, for providing a supportive research environment. The research leading to these results has received funding from QuantERA Grant No.

ANR-22-QUA2-000801 (MENTA) and ANR Grant No. 20-CE-47-0001-01 (COSQUA), the LabEx PALM (ANR-10-LABX-0039PALM). V.G. acknowledges the Région Ile-de-France in the framework of the DIM SIRTEQ program and the Quantum Saclay program FQPS (ANR-21-CMAQ-0002). R.D. acknowledges a PhD grant with reference 2024.03181.BD from the Portuguese Foundation for Science and Technology (FCT). S.R. is funded by the CNRS Chair in Physical Hydrodynamics (ANR-22-CPJ2-0039-01).

* victor.gondret@normalesup.org

† Present address Qblox, Delftechpark, Netherlands.

‡ denis.boiron@institutoptique.fr

§ christopher.westbrook@institutoptique.fr

- [1] S. W. Hawking, Black hole explosions?, *Nature* **248**, 30 (1974).
- [2] V. F. Mukhanov and G. V. Chibisov, Quantum fluctuations and a nonsingular universe, *ZhETF Pisma Redaktsiiu* **33**, 549 (1981).
- [3] L. Kofman, A. Linde, and A. A. Starobinsky, Towards the theory of reheating after inflation, *Phys. Rev. D* **56**, 3258 (1997).
- [4] W. G. Unruh, Experimental black-hole evaporation?, *Phys. Rev. Lett.* **46**, 1351 (1981).
- [5] D. Campo and R. Parentani, Inflationary spectra and violations of Bell inequalities, *Phys. Rev. D* **74**, 025001 (2006).
- [6] A. Micheli, *Entanglement and Decoherence in Cosmology and in Analogue Gravity Experiments*, Ph.D. thesis, Université Paris-Saclay (2023), [arXiv:2412.02444 \[gr-qc\]](https://arxiv.org/abs/2412.02444).
- [7] T. G. Philbin, C. Kuklewicz, S. Robertson, S. Hill, F. König, and U. Leonhardt, Fiber-optical analog of the event horizon, *Science* **319**, 1367 (2008).
- [8] S. Weinfurter, E. W. Tedford, M. C. J. Penrice, W. G. Unruh, and G. A. Lawrence, Measurement of stimulated Hawking emission in an analogue system, *Phys. Rev. Lett.* **106**, 021302 (2011).
- [9] J. Steinhauer, Observation of quantum Hawking radiation and its entanglement in an analogue black hole, *Nature Physics* **12**, 959 (2016).
- [10] L.-P. Euvé, F. Michel, R. Parentani, T. G. Philbin, and G. Rousseaux, Observation of noise correlated by the Hawking effect in a water tank, *Phys. Rev. Lett.* **117**, 121301 (2016).
- [11] J. Drori, Y. Rosenberg, D. Bermudez, Y. Silberberg, and U. Leonhardt, Observation of stimulated Hawking radiation in an optical analogue, *Phys. Rev. Lett.* **122**, 010404 (2019).
- [12] J. R. Muñoz De Nova, K. Golubkov, V. I. Kolobov, and J. Steinhauer, Observation of thermal Hawking radiation and its temperature in an analogue black hole, *Nature* **569**, 688 (2019).
- [13] K. Falque, A. Delhom, Q. Glorieux, E. Giacobino, A. Bramati, and M. J. Jacquet, Polariton fluids as quantum field theory simulators on tailored curved spacetimes, *Phys. Rev. Lett.*, (2025).
- [14] S. Eckel, A. Kumar, T. Jacobson, I. B. Spielman, and G. K. Campbell, A rapidly expanding Bose-Einstein condensate: An expanding universe in the lab, *Phys. Rev. X* **8**, 021021 (2018).
- [15] C. M. Wilson, G. Johansson, A. Pourkabirian, M. Simoen, J. R. Johansson, T. Duty, F. Nori, and P. Delsing, Observation of the dynamical Casimir effect in a superconducting circuit, *Nature* **479**, 376 (2011).
- [16] J. Hu, L. Feng, Z. Zhang, and C. Chin, Quantum simulation of Unruh radiation, *Nature Physics* **15**, 785 (2019).
- [17] M. Sparn, E. Kath, N. Liebster, J. Duchene, C. F. Schmidt, M. Tolosa-Simeón, A. Parra-López, S. Floerchinger, H. Strobel, and M. K. Oberthaler, Experimental particle production in time-dependent spacetimes: A one-dimensional scattering problem, *Phys. Rev. Lett.* **133**, 260201 (2024).
- [18] A. Zenesini, A. Berti, R. Cominotti, C. Rogora, I. G. Moss, T. P. Billam, I. Carusotto, G. Lamporesi, A. Recati, and G. Ferrari, False vacuum decay via bubble formation in ferromagnetic superfluids, *Nature Physics* **20**, 558 (2024).
- [19] C. Barceló, S. Liberati, and M. Visser, Analogue Gravity, *Living reviews in relativity* **14**, 1 (2011).
- [20] C.-A. Chen, S. Khlebnikov, and C.-L. Hung, Observation of quasiparticle pair production and quantum entanglement in atomic quantum gases quenched to an attractive interaction, *Phys. Rev. Lett.* **127**, 060404 (2021).
- [21] A. Tenart, G. Hercé, J.-P. Bureik, A. Dareau, and D. Clément, Observation of pairs of atoms at opposite momenta in an equilibrium interacting Bose gas, *Nature Physics* **17**, 1364 (2021).
- [22] P. Lähteenmäki, G. S. Paraoanu, J. Hassel, and P. J. Hakonen, Dynamical Casimir effect in a Josephson metamaterial, *Proceedings of the National Academy of Sciences* **110**, 4234 (2013).
- [23] S. Vezzoli, A. Mussot, N. Westerberg, A. Kudlinski, H. Dinparasti Saleh, A. Prain, F. Biancalana, E. Lantz, and D. Facio, Optical analogue of the dynamical Casimir effect in a dispersion-oscillating fibre, *Communications Physics* **2**, 84 (2019).
- [24] P. Engels, C. Atherton, and M. A. Hoefer, Observation of Faraday waves in a Bose-Einstein condensate, *Phys. Rev. Lett.* **98**, 095301 (2007).
- [25] J. H. V. Nguyen, M. C. Tsatsos, D. Luo, A. U. J. Lode, G. D. Telles, V. S. Bagnato, and R. G. Hulet, Parametric excitation of a Bose-Einstein condensate: From Faraday waves to granulation, *Phys. Rev. X* **9**, 011052 (2019).
- [26] D. Hernández-Rajkov, J. E. Padilla-Castillo, A. del Río-Lima, A. Gutiérrez-Valdés, F. J. Poveda-Cuevas, and J. A. Seman, Faraday waves in strongly interacting superfluids, *New Journal of Physics* **23**, 103038 (2021).
- [27] N. Liebster, M. Sparn, E. Kath, J. Duchene, K. Fujii, S. L. Görlitz, T. Enss, H. Strobel, and M. K. Oberthaler, Observation of pattern stabilization in a driven superfluid, *Phys. Rev. X* **15**, 011026 (2025).
- [28] J.-C. Jaskula, G. B. Partridge, M. Bonneau, R. Lopes, J. Ru-audel, D. Boiron, and C. I. Westbrook, Acoustic analog to the dynamical Casimir effect in a Bose-Einstein condensate, *Phys. Rev. Lett.* **109**, 220401 (2012).
- [29] L. W. Clark, A. Gaj, L. Feng, and C. Chin, Collective emission of matter-wave jets from driven Bose-Einstein condensates, *Nature* **551**, 356 (2017).
- [30] V. Gondret, C. Lamirault, R. Dias, C. Leprince, C. I. Westbrook, D. Clément, and D. Boiron, *Quantifying two-mode entanglement of bosonic Gaussian states from their full counting statistics* (2025), [arXiv:2503.09555 \[quant-ph\]](https://arxiv.org/abs/2503.09555).
- [31] G. B. Partridge, J.-C. Jaskula, M. Bonneau, D. Boiron, and C. I. Westbrook, Bose-Einstein condensation and spin mixtures of optically trapped metastable helium, *Phys. Rev. A* **81**, 053631 (2010).
- [32] L. Pitaevskii and S. Stringari, *Bose-Einstein condensation and superfluidity* (Oxford University Press, 2016).
- [33] X. Busch, R. Parentani, and S. Robertson, Quantum entanglement due to a modulated dynamical Casimir effect, *Phys. Rev. A* **89**, 063606 (2014).
- [34] S. Butera, D. Clément, and I. Carusotto, Position- and momentum-space two-body correlations in a weakly interact-

- ing trapped condensate, *Phys. Rev. A* **103**, 013302 (2021).
- [35] F. Gerbier, Quasi-1D Bose-Einstein condensates in the dimensional crossover regime, *Europhysics Letters* **66**, 771 (2004).
- [36] F. Chevy, V. Bretin, P. Rosenbusch, K. W. Madison, and J. Dalibard, Transverse breathing mode of an elongated Bose-Einstein condensate, *Phys. Rev. Lett.* **88**, 250402 (2002).
- [37] B. Jackson and E. Zaremba, Accidental suppression of Landau damping of the transverse breathing mode in elongated Bose-Einstein condensates, *Phys. Rev. Lett.* **89**, 150402 (2002).
- [38] C. Tozzo and F. Dalfovo, Phonon evaporation in freely expanding Bose-Einstein condensates, *Phys. Rev. A* **69**, 053606 (2004).
- [39] S. Robertson, F. Michel, and R. Parentani, Controlling and observing nonseparability of phonons created in time-dependent 1D atomic Bose condensates, *Phys. Rev. D* **95**, 065020 (2017).
- [40] C. Lepince, V. Gondret, C. Lamirault, R. Dias, Q. Marolleau, D. Boiron, and C. I. Westbrook, Coherent coupling of momentum states: Selectivity and phase control, *Phys. Rev. A* **111**, 063304 (2025).
- [41] M. Schellekens, R. Hoppeler, A. Perrin, J. V. Gomes, D. Boiron, A. Aspect, and C. I. Westbrook, Hanbury Brown Twiss effect for ultracold quantum gases, *Science* **310**, 648 (2005).
- [42] The region Ω takes into account all atoms within a volume $[-40, -8] \cup [8, 40]$ mm/s along v_z and $[-40, 40]$ mm/s along v_x and v_y . The plot shows $g_a^{(2)}(\delta v_z) = \iint_{-\Delta_\perp/2}^{\Delta_\perp/2} g^{(2)}(\delta \mathbf{v}) d\delta v_{x,y}^2$ with a transverse integration of $\Delta_\perp = 2\sigma_\perp$.
- [43] J. V. Gomes, A. Perrin, M. Schellekens, D. Boiron, C. I. Westbrook, and M. Belsley, Theory for a Hanbury Brown Twiss experiment with a ballistically expanding cloud of cold atoms, *Phys. Rev. A* **74**, 053607 (2006).
- [44] B. Yurke and M. Potasek, Obtainment of thermal noise from a pure quantum state, *Phys. Rev. A* **36**, 3464 (1987).
- [45] M. Perrier, Z. Amodjee, P. Dussarrat, A. Dareau, A. Aspect, M. Cheneau, D. Boiron, and C. I. Westbrook, Thermal counting statistics in an atomic two-mode squeezed vacuum state, *SciPost Phys.* **7**, 002 (2019).
- [46] M. Kardar, *Statistical Physics of Fields* (Cambridge University Press, 2007) Chap. 5.
- [47] A. Avagyan, E. Knill, and S. Glancy, Multi-mode Gaussian state analysis with total-photon counting, *Journal of Physics B: Atomic, Molecular and Optical Physics* **56**, 145501 (2023).
- [48] The population is rescaled by the factor $\prod_i \text{erf}(\Delta v_i / 2\sqrt{2}\sigma_i)$ (with $i = x, y, z$) to account for the fact that the voxels do not include all the atoms in each mode.
- [49] J. Martin, A. Micheli, and V. Vennin, Discord and decoherence, *Journal of Cosmology and Astroparticle Physics* **2022** (04), 051.
- [50] S. Robertson, F. Michel, and R. Parentani, Assessing degrees of entanglement of phonon states in atomic Bose gases through the measurement of commuting observables, *Phys. Rev. D* **96**, 045012 (2017).
- [51] J.-C. Jaskula, M. Bonneau, G. B. Partridge, V. Krachmalnicoff, P. Deuar, K. V. Kheruntsyan, A. Aspect, D. Boiron, and C. I. Westbrook, Sub-Poissonian number differences in four-wave mixing of matter waves, *Phys. Rev. Lett.* **105**, 190402 (2010).
- [52] K. V. Kheruntsyan, J.-C. Jaskula, P. Deuar, M. Bonneau, G. B. Partridge, J. Ruaudel, R. Lopes, D. Boiron, and C. I. Westbrook, Violation of the Cauchy-Schwarz inequality with matter waves, *Phys. Rev. Lett.* **108**, 260401 (2012).
- [53] Since the mode populations are equal, a normalized variance below unity directly signals a violation of the classical Cauchy-Schwarz inequality [62]. Assuming that the particles are identical bosons, this violation also reveals *particle* entanglement between the quasiparticles [63].
- [54] A. Micheli and S. Robertson, Phonon decay in one-dimensional atomic Bose quasicondensates via Beliaev-Landau damping, *Phys. Rev. B* **106**, 214528 (2022).
- [55] The growth will be discussed in more detail in a future publication.
- [56] A. Micheli and S. Robertson, Dissipative parametric resonance in a modulated 1D Bose gas, *Comptes Rendus Physique* **25**, 1 (2024).
- [57] S. Robertson, F. Michel, and R. Parentani, Nonlinearities induced by parametric resonance in effectively 1D atomic Bose condensates, *Phys. Rev. D* **98**, 056003 (2018).
- [58] S. M. D. Gregory, S. Schiattarella, V. S. Barroso, D. I. Kaiser, A. Avgoustidis, and S. Weinfurter, *Tracking the nonlinear formation of an interfacial wave spectral cascade from one to few to many* (2025), [arXiv:2410.08842 \[gr-qc\]](https://arxiv.org/abs/2410.08842).
- [59] T. Schweigler, M. Gluza, M. Tajik, S. Sotiriadis, F. Cataldini, S.-C. Ji, F. S. Møller, J. Sabino, B. Rauer, J. Eisert, and J. Schmiedmayer, Decay and recurrence of non-Gaussian correlations in a quantum many-body system, *Nature Physics* **17**, 559 (2021).
- [60] J.-P. Bureik, G. Hercé, M. Allemand, A. Tenart, T. Roscilde, and D. Clément, Suppression of Bogoliubov momentum pairing and emergence of non-Gaussian correlations in ultracold interacting Bose gases, *Nature Physics* **21**, 57 (2025).
- [61] V. Gondret, C. Lamirault, R. Dias, L. Camier, D. Boiron, and C. Westbrook, Data for the paper entitled "observation of entanglement in a cold atom analog of cosmological preheating", [10.5281/zenodo.15747622](https://zenodo.org/record/15747622) (2025).
- [62] A. Finke, P. Jain, and S. Weinfurter, On the observation of non-classical excitations in bose-einstein condensates, *New Journal of Physics* **18**, 113017 (2016).
- [63] T. Wasak, P. Szańkowski, P. Ziń, M. Trippenbach, and J. Chwedeńczuk, Cauchy-Schwarz inequality and particle entanglement, *Phys. Rev. A* **90**, 033616 (2014).
- [64] R. Lopes, A. Imanaliev, A. Aspect, M. Cheneau, D. Boiron, and C. I. Westbrook, Atomic Hong-Ou-Mandel experiment, *Nature* **520**, 66 (2015).
- [65] S. Kannan, Y. S. Athreya, A. H. Abbas, X. T. Yan, S. S. Hodgman, and A. G. Truscott, Measurement of the s-wave scattering length between metastable helium isotopes, *Phys. Rev. A* **110**, 063324 (2024).
- [66] L. Mandel and E. Wolf, *Optical coherence and quantum optics* (Cambridge university press, 1995).
- [67] P. Błasiak, A. Horzela, K. A. Penson, A. I. Solomon, and G. H. E. Duchamp, Combinatorics and boson normal ordering: A gentle introduction, *American Journal of Physics* **75**, 639 (2007).

End matter

Detector quantum efficiency

An accurate estimate of the quantum efficiency of the MCP detector is difficult. Earlier work on similar detectors on metastable helium yielded values ranging from 20% to 50% [21, 64, 65]. For plotting purposes, we take 25(5)%, compatible with the estimation made on our own detector. Since the entanglement witness depends on a normalized correlator, it depends very little on the exact value of the quantum efficiency. A higher quantum efficiency would shift the

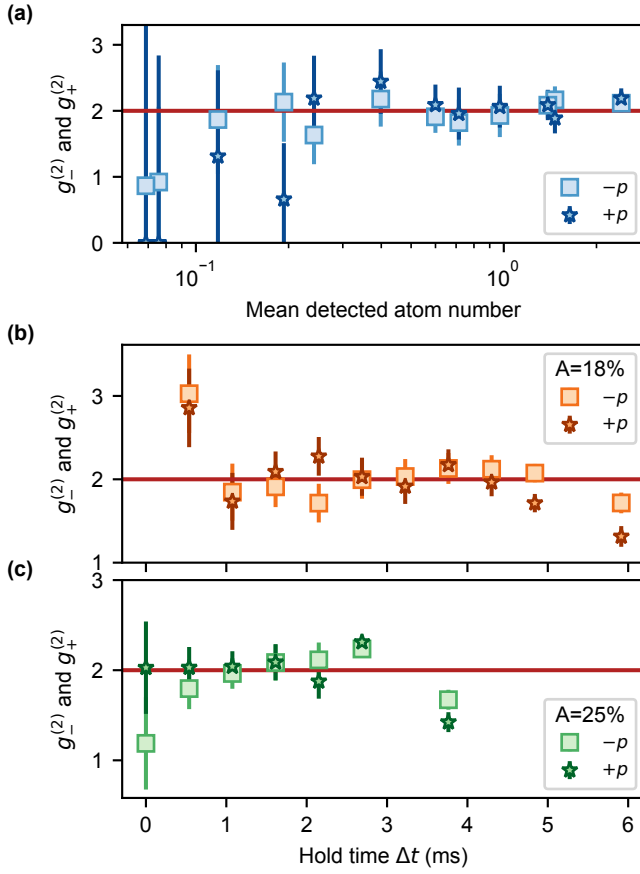


FIG. 4. (a) The auto-correlator computed with the same dataset as in Fig. 2, in which we vary the modulation depth for a constant hold time. Panels (b) and (c) show the corresponding auto-correlator for the dataset of Fig. 3 where the hold time is varied with a modulation depth of respectively 18% and 25%. The light square markers show the negative velocity sideband and the dark stars the positive velocity one. The error bars are computed from the expected error for a thermal law with the same detected atom number.

entanglement witness curve of Fig. 2 to the right but even a quantum efficiency of 100% would not change our conclusion on entanglement.

Auto-correlations

For purposes of comparison, we show in Fig. 4 the normalized two-body auto-correlators for the same data as that we used for Figs. 2 and 3. The normalized two-body auto-correlators are defined as

$$g_j^{(2)} = \frac{G_j^{(2)}}{n_j^2} = \frac{\langle (\hat{a}_j^\dagger)^2 \hat{a}_j \rangle}{n_j^2} \quad (6)$$

where $j = +$ or $-$. These auto-correlators are always consistent with the value 2 except in the case of very weak or very strong excitation. For weak excitation, the number of atoms in the sidebands is very low, resulting in large error bars, that we discuss below. In addition, the signal in the voxels is contaminated by other residual atoms. In the case of strong excitation,

the decrease in the correlation may indicate a non-Gaussian state.

The error bars shown in Fig. 4 are not obtained using bootstrap techniques, but are instead estimated based on the number of repetitions and the mean detected atom number in the voxels. When the population is sufficiently large, this estimation yields results consistent with a bootstrap analysis. However, when the mean detected atom number is very low, the available statistics are insufficient to reliably estimate error bars. In some cases, for instance, no doublets are recorded at all, due to limited statistics. Thus, the error bars on $g^{(d)}$ are given by

$$\Delta g^{(d)} = \frac{d!}{\sqrt{N_{\text{shot}}}} \sqrt{\frac{\text{Var}[(\hat{a}_j^\dagger)^d \hat{a}_j^d]}{[(d!)n^d]^2} + d \frac{\text{Var}[\hat{a}_j^\dagger \hat{a}_j]}{n^2}} \quad (7)$$

where the variance is evaluated using Eq. (11) only depends on the mean detected atom number and N_{shot} is the number of experimental cycles. Here $d!$ represents the value of $g^{(d)}$ for a thermal statistics.

In the following, we derive Eq. (11) for a state with a thermal statistics. To do so, we need to evaluate

$$\text{Var}[(\hat{a}^\dagger)^d \hat{a}^d] = \langle (\hat{a}^\dagger)^d \hat{a}^d (\hat{a}^\dagger)^d \hat{a}^d \rangle - \langle (\hat{a}^\dagger)^d \hat{a}^d \rangle^2 \quad (8)$$

where we drop the label j to lighten notations. The second term in Eq. (8) is the d -body auto-correlator which is given by $G^{(d)} = \langle (\hat{a}^\dagger)^d \hat{a}^d \rangle = (d!)n^d$ in the case of a thermal statistics [66]. To evaluate the first term, we normal order the creation and annihilation operators as [67]

$$\begin{aligned} (\hat{a}^\dagger)^d \hat{a}^d (\hat{a}^\dagger)^d \hat{a}^d &= \underbrace{:(\hat{a}^\dagger)^d \hat{a}^d (\hat{a}^\dagger)^d \hat{a}^d:}_{\text{no pair removed}} \\ &+ \underbrace{:(\hat{a}^\dagger)^d \hat{a}^{d-1} (\hat{a}^\dagger)^{d-1} \hat{a}^d:}_{\text{remove 1 pair}} \times \underbrace{\binom{d}{1} \times \binom{d}{1}}_{\text{\# of pairs}} \\ &+ \underbrace{:(\hat{a}^\dagger)^d \hat{a}^{d-2} (\hat{a}^\dagger)^{d-2} \hat{a}^d:}_{\text{remove 2 pairs}} \times \underbrace{\binom{d}{2} \times \binom{d}{2} \times 2}_{\text{choose } \hat{a} \text{ then } \hat{a}^\dagger, \text{ pair them}} \\ &+ \underbrace{:(\hat{a}^\dagger)^d \hat{a}^{d-3} (\hat{a}^\dagger)^{d-3} \hat{a}^d:}_{\text{remove 3 pairs}} \times \underbrace{\binom{d}{3} \times \binom{d}{3} \times 3 \times 2}_{\text{choose } \hat{a} \text{ then } \hat{a}^\dagger, \text{ pair them}} + \dots \end{aligned} \quad (9)$$

from which we obtain

$$\langle (\hat{a}^\dagger)^d \hat{a}^d (\hat{a}^\dagger)^d \hat{a}^d \rangle = \sum_{k=0}^d k! \binom{d}{k}^2 G^{(2d-k)}. \quad (10)$$

We therefore have

$$\text{Var}[(\hat{a}^\dagger)^d \hat{a}^d] = \sum_{k=0}^d k! \binom{d}{k}^2 (2d-k)! n^{2d-k} - [d! n^d]^2. \quad (11)$$